PAPER

Surface modification of closed cell titanium foam through electrical discharge texturing

To cite this article: Adithya V *et al* 2025 *Phys. Scr.* **100** 055007

Physica Scripta

PAPER

Surface modification of closed cell titanium foam through electrical discharge texturing

RECEIVED
11 November 2024

REVISED
19 March 2025

ACCEPTED FOR PUBLICATION
31 March 2025

PUBLISHED
9 April 2025

Adithya V[1], **Bharath P**[1], **Ashwin Polishetty**[2] **and Giridharan Abimannan**[1]

[1] School of Mechanical Engineering, Vellore Institute of Technology Chennai, Tamilnadu—600127, India
[2] School of Engineering, Auckland University of Technology, Auckland, NZ 1142, New Zealand

E-mail: giridharan.abimannan@vit.ac.in

Keywords: DSEDT, titanium foam, crater diameter, Re-solidified layer, EDS profile

Abstract

In this paper, the Die-Sinker Electrical Discharge Texturing (DSEDT) is utilized to machine closed cell titanium foam using pure brass tool electrode. Discharge time, current and discharge voltage were taken as input factors. By varying these input factors, discharge energy generated in between the tool and workpiece gets altered. Therefore, the influence of discharge energy on the average crater diameter, re-solidified layer thickness and chemical alteration of machined surface are analysed. The stochastic nature of DSEDT process is studied using microscopic images and energy dispersive x-ray spectroscopy profiles. Through micrographs it is perceived, increase in the discharge energy from 5.12 J to 10.13 J, leads to an increase in average crater diameter from 29.26 to 66.29 μm respectively. It is observed that combined effect of crater overlap phenomena and re-solidification of material seals the cells in a foam material. A minimum re-solidified layer thickness of 44.29 μm is achieved. The machined surface of closed cell titanium foam shows significant rise in carbon, copper and zinc elements owing to the disintegration of the dielectric liquid and tool electrode during spark erosion. The study on DSEDT of closed cell titanium foam revealed the possibility to create surfaces with uniform crater diameter and establish titanium carbide on the machined surface.

1. Introduction

Process induced surfaces are generated on components top layer to improve its lubrication, heat transfer characteristics, bio-compatibility and polarity characteristics. The use of light in weight materials are adopted in aviation and automotive industries owed to the stringent requirements to reduce fuel consumption and minimal carbon footprints. By 2030, the use of lightweight materials in aerospace and automotive industry is expected to rise up to 85% and 70% respectively [1]. Metal foams can be used to meet the sudden rise in demand for lightweight materials in both industries. Metal foams are classified as open cell foam composed of interconnected pores and closed foam contains isolated pores which are not interconnected. Service life can be enhanced by altering the surface of metal foam components. Surface modification of metal foams through traditional machining techniques is not recommended as the cutting force exerted by the tool upon foam workpiece may damage or collapse the cellular arrangement owed to smearing effect. Non-traditional machining techniques using laser, electrolytic processing, chemical etching and Electrical Discharge Machining (EDM) are the most frequently adopted in industry's to machine metal foams. However, the protrusions left by laser, poor control of electrolytic process and uneven texture surface produced by etchants have limited the use of these techniques. EDM is increasingly being used in industries to machine metallic foams since the force produced in EDM is trivial and the texture produced on the machined surface do not contain directional properties. Die-Sinker Electrical Discharge Texturing (DSEDT), a subtractive machining method that works on the principle of EDM is employed to generate random and isotropic textures on electrically conductive material regardless of their hardness. In a DSEDT process, texturing is achieved by giving the least depth of cut to the workpiece which leads to texturing instead of machining. Use of metal foams as sandwich design panels offer

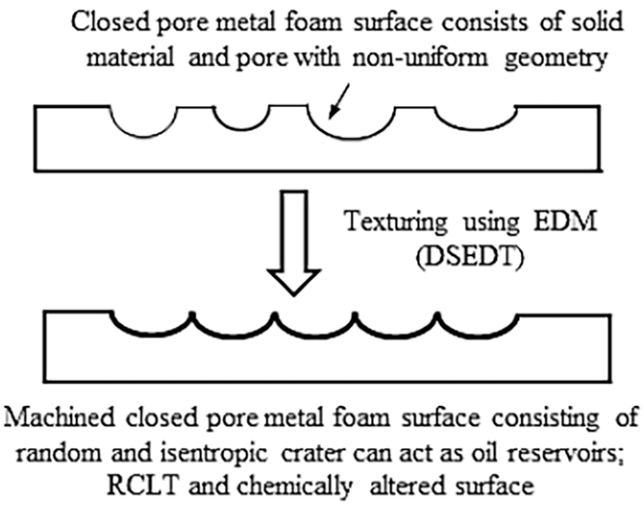

Figure 1. DSEDT on CTF.

better protection against wear along with high stiffness as compare to bare foam. The existing foam preparation methods have limitation in achieving uniform pore geometry due to lack in control over manufacturing route (poor gas dispersion, etc). In this study closed pore metal foam is chosen as workpiece material. Closed pore foam is featured with non-uniform pore shapes which are not interconnected. Uniform pore geometry on metal foam components is desired as it can act as oil reservoirs or lubrication pockets. During DSEDT of closed pore metal foam, each pulse discharge produces a crater on the machined surface. As the spark discharge continues numerous individual craters along with overlapping craters are produced on the machined surface. As a result, random and isotropic craters are established on the machined surface which can act as oil reservoirs. The schematic representation of surfaces produced through DSEDT is presented in figure 1.

The initial work on texturing by EDM was attempted to create matt-finish on roll mill to reduce the adhesion of sheet metal to the roller surface [1]. Koshy and Tovey developed textures on rake face of cutting tools to promote lubricant retention during machining [2]. Harcuba *et al* used EDT to establish textures on orthopedic implants and stated that the EDT surface offered better biocompatibility [3]. Jithin *et al* for the first time revealed the possibility of using EDM as an alternate cost-effective technique to improve the wettability of SS 304 alloy through texturing [4]. He *et al* produced micro/nano textured surface through EDM which can be used for anti-fouling application [5].

Bui *et al* used silver suspended dielectric medium in EDM and established textured surfaces which offered better antibacterial property [6]. Wang *et al* used EDM together with electro deposition to create surface that showed super hydrophobic property [7]. Assessing the machinability of titanium foam using EDM process and evaluating the surface produced is the need of the hour for an industry, as the process witness marks/texture has direct influence on the useful life of the component. Many investigators have strived to grasp the witness marks left over by EDM technology while machining a variety of workpiece materials. Klink *et al* attempted to evaluate the crater morphology produced on tool steel material by using dissimilar power generators [8]. Authors proposed that the EDM power generators available today can generate widened and shallow crater profiles. The influence of EDM process parameters such as tool polarity, voltage, current and pulse time on crater formation during machining nickel-titanium material and GH4169 nickel-based alloy [9, 10] were explored. The authors proposed a hypothesis that the crater diameter widens for higher magnitudes of process parameters. By increasing the magnitude of pulse time, current and voltage, the discharge energy upsurge which produces enlarged and deeper crater that aids for enhanced hydrophobicity of EDM machined surface [9, 11–13]. Also, a reduction in crater overlap on EDM machined Ti6Al4V surface is noticed while using transesterified bio-oil as dielectric [14] and 25% normal water mixed dielectric liquid [15]. Authors have studied the influence of EDM process variables on re-solidified layer thickness (RLT) formed on materials such as Ni-Ti alloy [11], Nickel based alloy [12], Ti-5Al-2.5Sn [16], Ti6Al4V [14, 17] and Al-Mg–Ti alloy [18]. The chemical alteration on EDM machined surfaces [19, 20] were also assessed on Ti6Al4V [21], Cu-Ni-TiN [22] and green compacted TiC/Cu materials [23].

The existing literature articulates that little work is published in EDT of metals, EDM for machining open foam materials, surface modification, RLT, and chemical alteration on machined surface of materials ranging from steel to titanium alloys. Yet the EDT of closed foam, particularly titanium foam and its consequences are not revealed in detail. Energy monitoring is imperative in every manufacturing method. Owing to the stochastic nature of EDM process, among the total energy supplied, only a portion of energy exists in the discharge gap

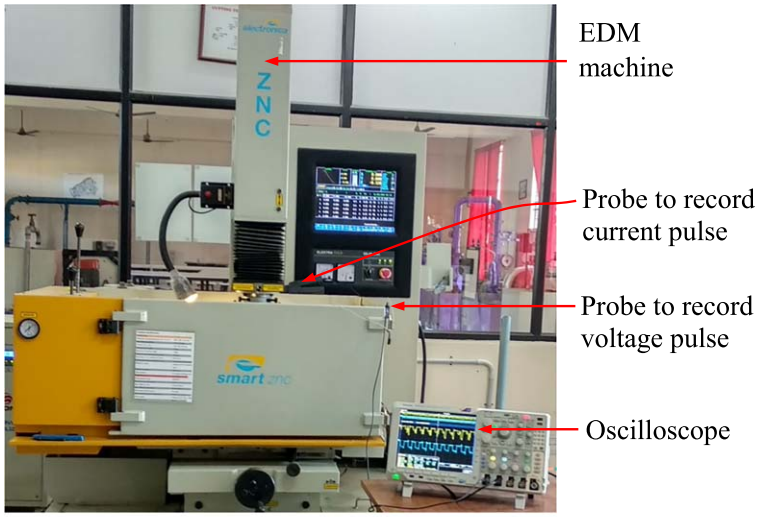

(a) Snapshot of setup used for the study

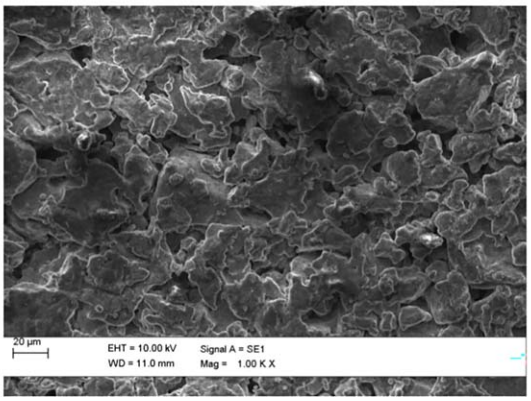

(b) SEM image of un-machined CTF (1000 X magnification)

Figure 2. Experimentation details.

[24]. However, the literature lacks quantifying the actual energy (or discharge energy) available in the discharge gap. EDT is achieved through formation of crater which is reliant on the energy available in the discharge gap. Titanium foams are ultra-light materials which are exclusively used in sound absorption, electron shielding and filters for aerospace application. In this study, the energy produced and the consequences of modifying the surface of closed pore titanium foam (CTF) during DSEDT are envisaged.

2. Materials and methods

A die-sinker EDM machine (Electronica smart ZNC) as shown in figure 2(a) is used for machining. CTF (99.87% pure confirmed by wet analysis) with 21% specific gravity [25] is taken as workpiece (100 mm × 100 mm × 2 mm) and a brass (ϕ 8 mm) is selected as tool electrode. The erosion of CTF took place inside a reservoir filled with hydrocarbon based dielectric liquid (ELEKTROL supplied by M/s. Electronica India Pvt Ltd). Among the various EDM process variables, discharge time (t_d), current (i_p), discharge voltage (v_g), duty factor, anti-arc sensitivity, polarity and dielectric flushing pressure shows dominant effect on the machinability of workpiece material [26]. Preliminary trials are conducted to identify the significant input parameter conditions. The process parameters t_d, i_p and v_g can be varied from 1 to 2000 µs; 0 to 60 A and 0 to 300 V respectively. To avoid rapid tool wear, the increasing discharge duration beyond 200 µs and current above 12 A was not selected. Furthermore, by machining tool connected to anode polarity and work piece to cathode polarity, tool wears severely. Consequently, experiments are conducted with cathode tool polarity and anode workpiece polarity. In this work, to modify the surface of CTF, the machine settings for experimentation are limited to finish machining regime. The selected workpiece is composed of closed cell and through the micrograph of SEM the average cell size is obtained as 5 µm. The setup utilized for experimentation and the

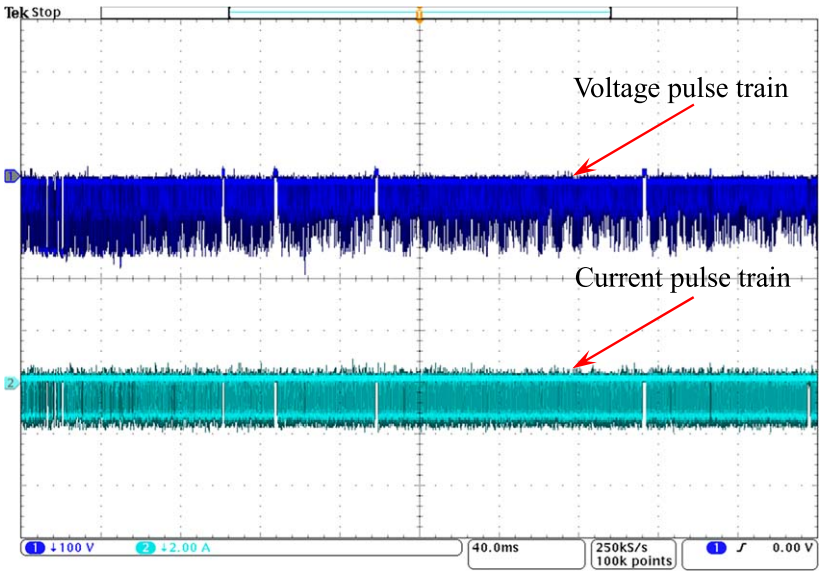

Figure 3. Typical voltage and current waveform captured for t_d-50 µs, i_p—6 A and v_g—60 V.

chosen workpiece are presented in figure 2. In this work, t_d, i_p and v_d are chosen as input factors. The surface produced by DSEDT is owed to the numerous random sparks occur between the electrodes. Discharge energy, topography, thickness of re-solidified layer (*RCLT*) and chemical alteration of machined surface are considered as outcomes. Dielectric flushing pressure, anti-arc sensitivity and duty factor are maintained constant at 1.5 kg cm^{-2}, 3 and Level 3 respectively. The input process variables are varied at four levels such as t_d - 50 µs, 100 µs, 150 µs, 200 µs; i_p - 6 A, 8 A, 10 A, 12 A and v_g - 30 V, 45 V, 60 V, 75 V.

A full factorial experiments (L64) is conducted by varying these input variables. For every combination of input process variables, the voltage and current waveforms (pulses) produced in the discharge gap is captured using a 4-channel oscilloscope with 5 Giga samples/s sampling rate. A HP9100 voltage probe and Tektronix A622 probe are used to record instantaneous voltage ($u(t)$) and instantaneous current ($i(t)$) respectively. Each pulse train data is captured for duration of 400 milliseconds with one lakh data points. A snapshot of pulse train recorded during machining is presented in figure 3. Using the acquired pulse train data, the discharge energy (E) is calculated using below expression [24, 27]

$$E = \int_0^{t_e} u(t)i(t)dt \tag{1}$$

where t_e—discharge time (or) effective machining time. The impact of input variables on E is investigated. The influence of E on topography, *RCLT,* chemical alteration, micro hardness, contact angle and surface roughness of machined component were also analyzed. For every combination of process variables, the micrographs of machined surfaces are captured at three distinct locales using SEM. Energy dispersive spectroscopy (EDS) profiles are used to reveal the chemical alteration built-up on the CTF machined surfaces by the EDM process. The surface roughness and micro-hardness of the machined surfaces are assessed using MarSurf GD 120 surface roughness tester and Shimadzu HMV Vickers hardness tester respectively. By changing the input variables, the E produced in the gap differs which alters the erosion phenomena discussed in subsequent sections.

3. Results

The influence of input factors (t_d, i_p, v_g) on discharge energy (E) is given in table 1. For each combination of input factors, experiments are conducted three times, and its mean value is presented in table 1. It is perceived that discharge energy increases with increase in t_d and i_p levels. For same i_p and v_g, as the t_d goes up, the discharge energy acquired in the gap upsurges. By increasing the t_d and i_p values, the energy for single pulse grows which results in higher discharge energy as shown in figure 4. However, for fixed duty factor, by raising the t_d magnitudes, a reduction in the frequency of pulses is noticed that caused lower E in the gap.

The drip in pulse frequency is perceived from the pulse train picked up for i_p - 8 A, v_g - 45 V and different t_d is shown in figure 5. During experimentation, the i_p is varied at 6, 8, 10 and 12 A. For all t_d and v_g, by raising the magnitude of i_p, negligible variation in current magnitudes generated in gap is witnessed. This is mainly attributed to the duty factor which is kept at level 3 (lower). The pulse duty factor varies the pulse off time in steps

Table 1. Significance of t_d, i_p, v_g on E.

Cutting trial	t_d	i_p	v_g	E	Cutting trial	t_d	ip	v_g	E
1			30	5.123	33			30	5.891
2		6	45	5.484	34		6	45	5.929
3			60	7.486	35			60	6.823
4			75	8.641	36			75	9.263
5	50		30	5.541	37			30	6.118
6		8	45	5.617	38		8	45	6.676
7			60	6.635	39			60	7.148
8			75	8.649	40			75	9.191
9			30	5.781	41	150		30	6.988
10		10	45	5.880	42		10	45	7.025
11			60	6.831	43			60	7.403
12			75	8.973	44			75	9.439
13			30	6.594	45			30	7.801
14		12	45	7.055	46		12	45	8.185
15			60	7.797	47			60	8.605
16			75	9.314	48			75	9.767
17			30	6.949	49			30	6.504
18		6	45	5.435	50		6	45	4.992
19			60	7.609	51			60	7.143
20			75	9.162	52			75	9.324
21			30	6.205	53	200		30	6.261
22		8	45	5.518	54		8	45	7.010
23			60	6.886	55			60	7.210
24			75	9.160	56			75	9.638
25	100		30	6.703	57			30	7.062
26		10	45	6.928	58		10	45	7.226
27			60	7.818	59			60	7.751
28			75	9.387	60			75	9.534
29			30	7.670	61			30	8.084
30		12	45	8.059	62		12	45	9.019
31			60	8.556	63			60	8.861
32			75	9.453	64			75	10.127

[ELECTRONICA Technology manual]. Though the magnitude of i_p grows from 6 A to 12 A as input, approximately 2 A to 3 A current is produced as output. The drop in current magnitude for varying i_p settings can be perceived from single current pulse picked up for t_d - 50 μs, v_g - 45 V and different i_p values as shown in figure 6. This brings about reduction in discharge energy for changing td and vg settings. It is witnessed from the above discussion that, by changing the input process variables the discharge energy (E) gets altered.

On the other hand, the machined surface of CTF gets altered due to deposition of recast layer (*RCLT*) and chemically as well owed to the pyrolysis effect of DSEDT. However, the diameter of crater, *RCLT* and metallurgical altered surface produced are dependent on the E produced in the spark gap. Therefore, the impact of E on the diameter of crater is analyzed first.

The consequence of varying E on topography of machined CTF surface is assessed using SEM captured at three distinct locations. It is perceived from figure 7, the machined surface of CTF contains crater and re-solidified molten material completely filling the pore which existed on the surface prior to machining. From the SEM images, the diameter of crater is evaluated using the Image J software and its average value ($C_{d.avg}$) is presented in figure 7. By varying the E from 5.12 J–9.53 J (low to high), the machined CTF contains $C_{d.avg}$ increasing from 29.26 μm–66.29 μm. Formation of crater on the CTF can be understood through the material removal mechanism of EDM process. In EDM, as the discharge begins and ends, material removal happens on both tool and workpiece (electrodes). Material removal from the electrodes occurs owed to melt and evaporation of electrodes by transformation of kinetic energy of ions and electrons into thermal energy. For a given E, as the discharge originates, the ions and electrons acquire kinetic energy and impinge upon the surface of electrodes causing melt, evaporation of electrodes and dielectric liquid as well that aids in formation of plasma surrounded by a compressed vapour bubble. As the discharge remains, owed to continuous melting and evaporation of electrodes and dielectric liquid, the plasma diameter and compressed vapour bubble grows. However the growth of the vapour bubble is restricted by the inertia of the surrounding dielectric liquid that leads to rise in pressure within the vapour bubble. At the end of discharge, the violent collapse of the plasma and vapour bubble causes the superheated molten liquid from the electrodes to expel into the dielectric liquid leaving a cavity or crater on the electrodes [28, 29]. The size of the crater formed is dependent

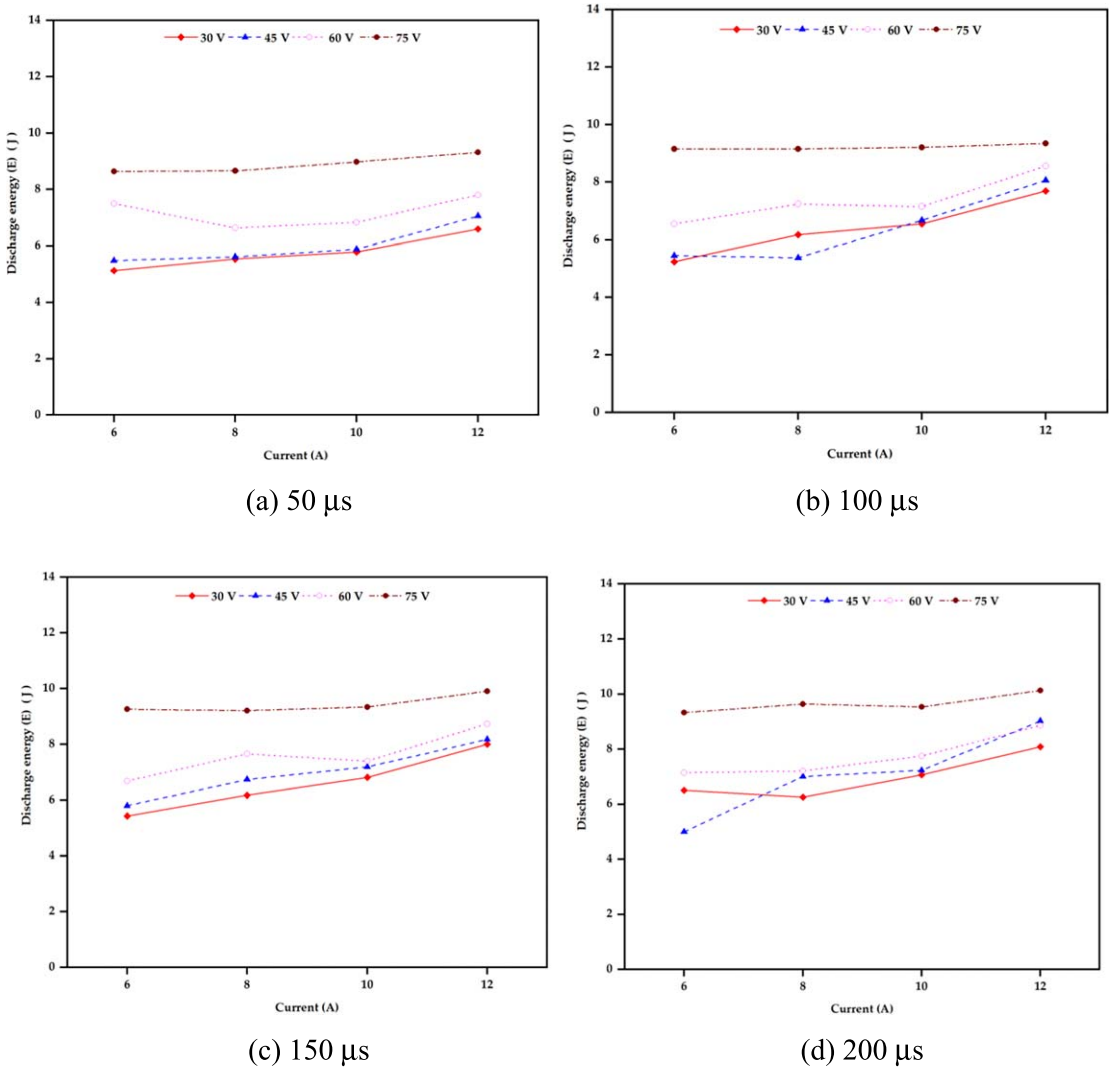

Figure 4. Impact of t_d, i_p, v_g on E.

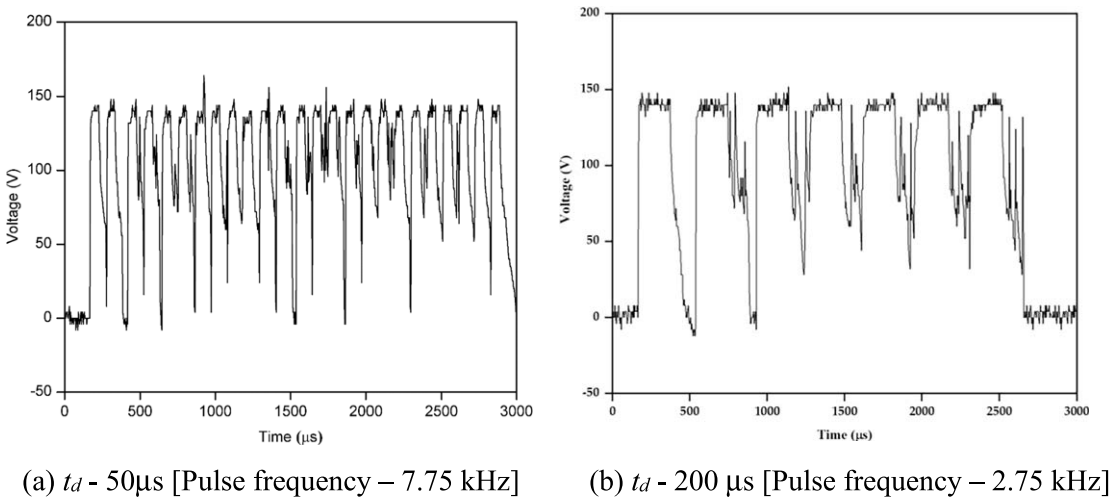

Figure 5. Voltage waveform acquired for i_p - 6 A and v_g - 60 V for varying t_d.

on the growth of plasma diameter. In this study the workpiece is connected to anode polarity, hence the effect of electrons is considered. At larger magnitudes of E, the density of electrons grows subsequently the melting and evaporation of electrodes that results in increased plasma diameter and vapour bubble [30]. At the end of

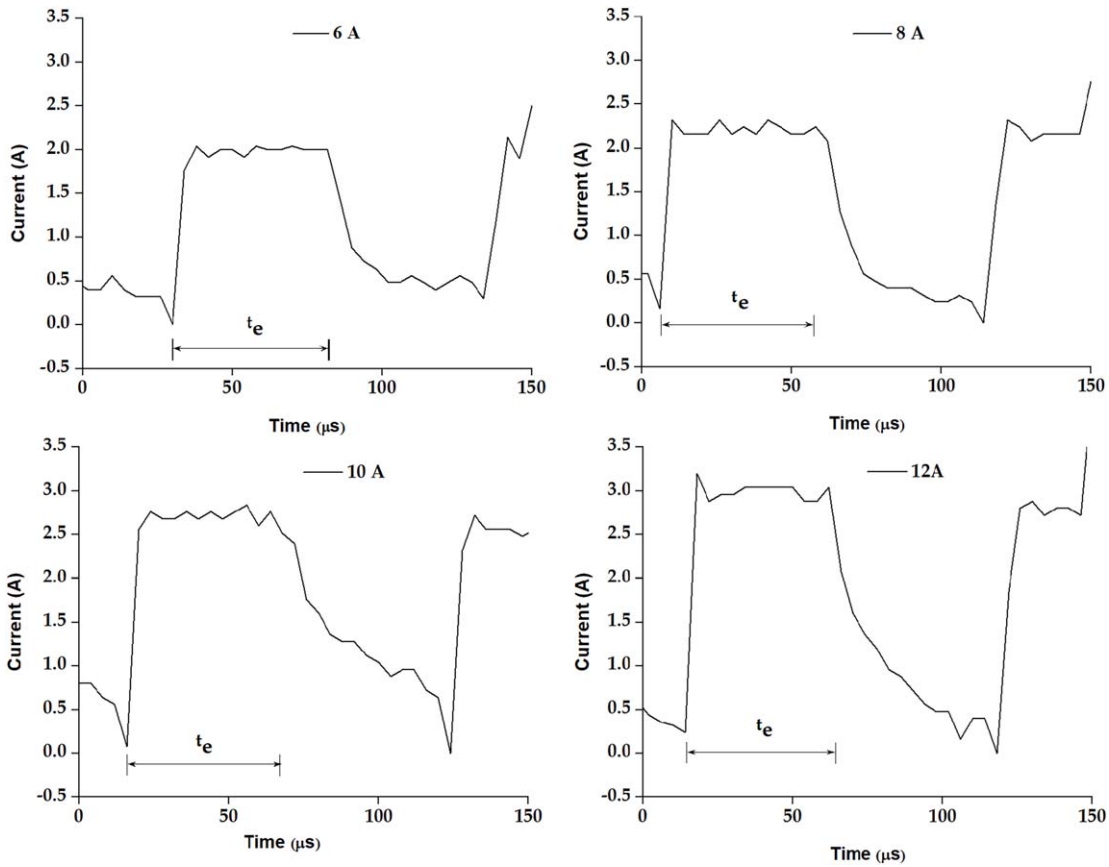

Figure 6. Individual current waveform acquired at t_d - 50 μs and v_g - 45 V for varying i_p.

discharge, the abrupt burst of plasma and vapour bubble ejects the molten liquid beneath the discharge vicinity forming larger size crater on the surface of workpiece. Through SEM images it is perceived, as the *E* raises, the machined surface of CTF contains random individual craters along with overlapping craters. Uniform crater diameter is observed on surfaces machined with *E* at 5.12 J, 6.64 J, 7.01 J, 9.16 J and 9.53 J. This shows that, DSEDT can be used for generating craters having uniform diameter which can act as lubrication pockets on machined surface. However crater overlapping, debris accumulation within the crater and spherical globules are also observed on the surfaces machined with varying *E* magnitudes. Owing to the continuous erosion and stochastic nature of EDM process, crater overlap is noticed. However, the workpiece contains closed cells, when the spark erosion occurs in region close to or upon the cell, this might result in crater overlap phenomenon. Also, the accumulation of debris into the crater is noticed on surfaces machined with *E* at 5.62 J, 6.64 J, 7.01 J and 9.53 J. In addition to the explanation given earlier, when the *E* grows, owing to the increased intensity of electro-thermal heating, the diameter of the compressed vapour bubble grows and more heat transfers into the workpiece by conduction [31]. This resulted in a larger crater diameter formed on machined surface. The un-ejected melted material re-deposit back on to the adjacent regions and seals the cells of CTF, which is noticed in figure 7.

Further analysis is carried out to understand the influence of *E* on *RCLT* and possible chemical alteration of CTF machined surface. Figure 8 presents the SEM micrograph revealing the re-solidified layer of machined workpiece for different *E*. At *E* - 5.12 J, owing to less intense *E*, smaller amount of material gets melted and the un-ejected melted material deposit onto the adjacent regions. This resulted in lower *RCLT* (44.29 μm) as shown in figure 8(a). In this study, the workpiece is maintained at anode polarity. During DSEDT machining, for fixed inter electrode gap, the energy distribution to anode workpiece is higher compared to that of cathode in hydrocarbon based dielectric. Also the heat transfer within the workpiece is mostly by conduction [31]. In EDM, the material removal efficiency or plasma flushing efficiency (PFE) is defined as the ratio of ejected to melted volume. It is reported in the literatures that the experimentally measured PFE ranges from 1–10% [32]. At higher magnitudes of *E* (10.13 J), more volume of molten material is generated compared to that formed with 5.12 J. Owed to the stochastic nature of EDM process crater overlap phenomena exist on the machined surface. The combined effect of poor *PFE*, crater overlap phenomena and stochastic nature of EDM process attributed to form thicker non-uniform *RCLT* (110.71 μm) on the machined surface as shown in figure 8(j). At lower *E* magnitudes the *RCLT* appears to be uniform whereas it becomes uneven as the *E* grows.

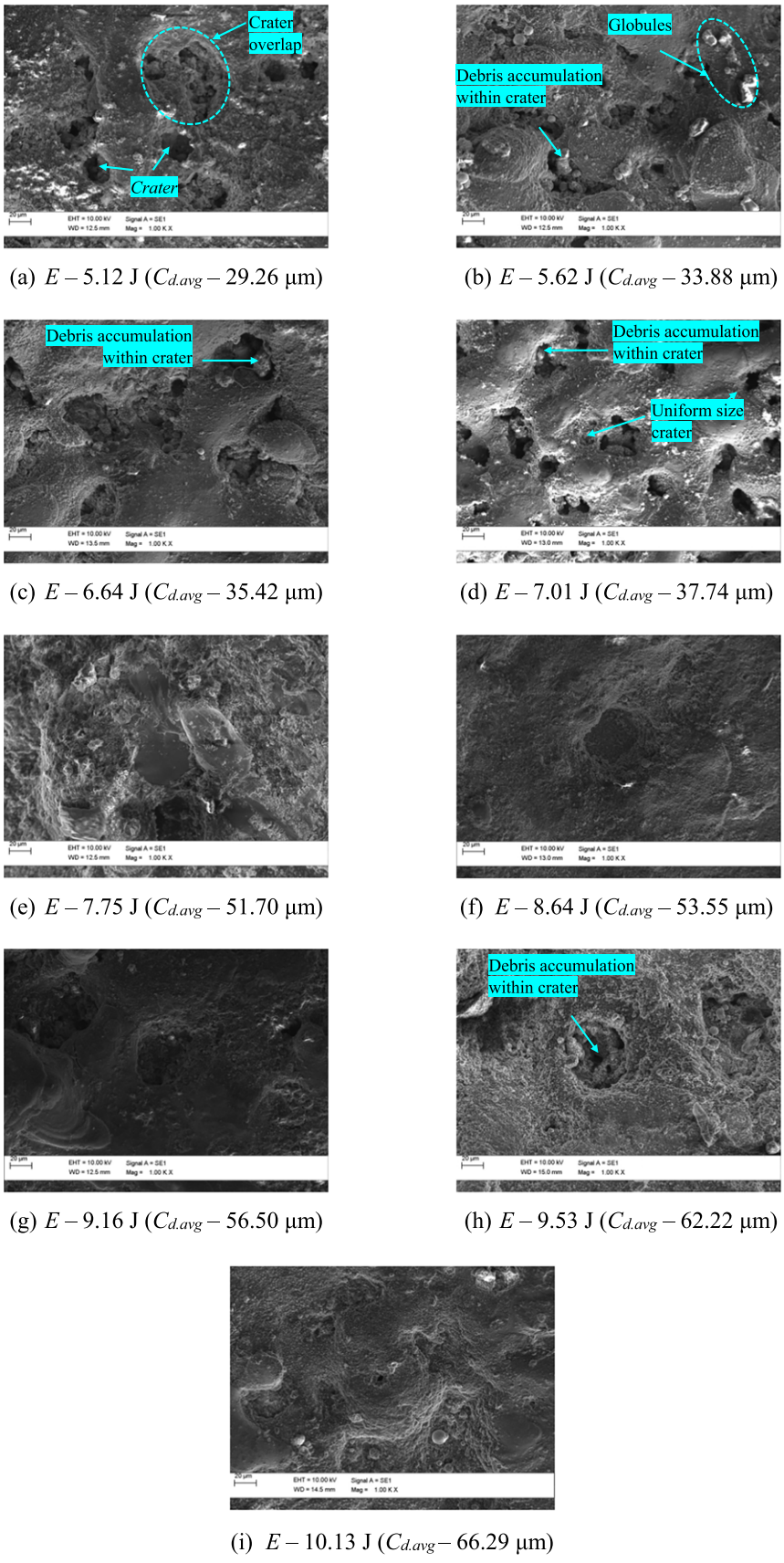

(a) E – 5.12 J ($C_{d.avg}$ – 29.26 µm) (b) E – 5.62 J ($C_{d.avg}$ – 33.88 µm)

(c) E – 6.64 J ($C_{d.avg}$ – 35.42 µm) (d) E – 7.01 J ($C_{d.avg}$ – 37.74 µm)

(e) E – 7.75 J ($C_{d.avg}$ – 51.70 µm) (f) E – 8.64 J ($C_{d.avg}$ – 53.55 µm)

(g) E – 9.16 J ($C_{d.avg}$ – 56.50 µm) (h) E – 9.53 J ($C_{d.avg}$ – 62.22 µm)

(i) E – 10.13 J ($C_{d.avg}$ – 66.29 µm)

Figure 7. Effect of E on $C_{d.avg}$.

The impact of E on chemical alteration of machined work piece is also analyzed. In DSEDT, spark erosion occur in-between the electrodes completely engulfed inside a dielectric liquid (a hydrocarbon based liquid). During spark discharge, a melted pool is generated at the surface of both tool and workpiece. The dielectric used

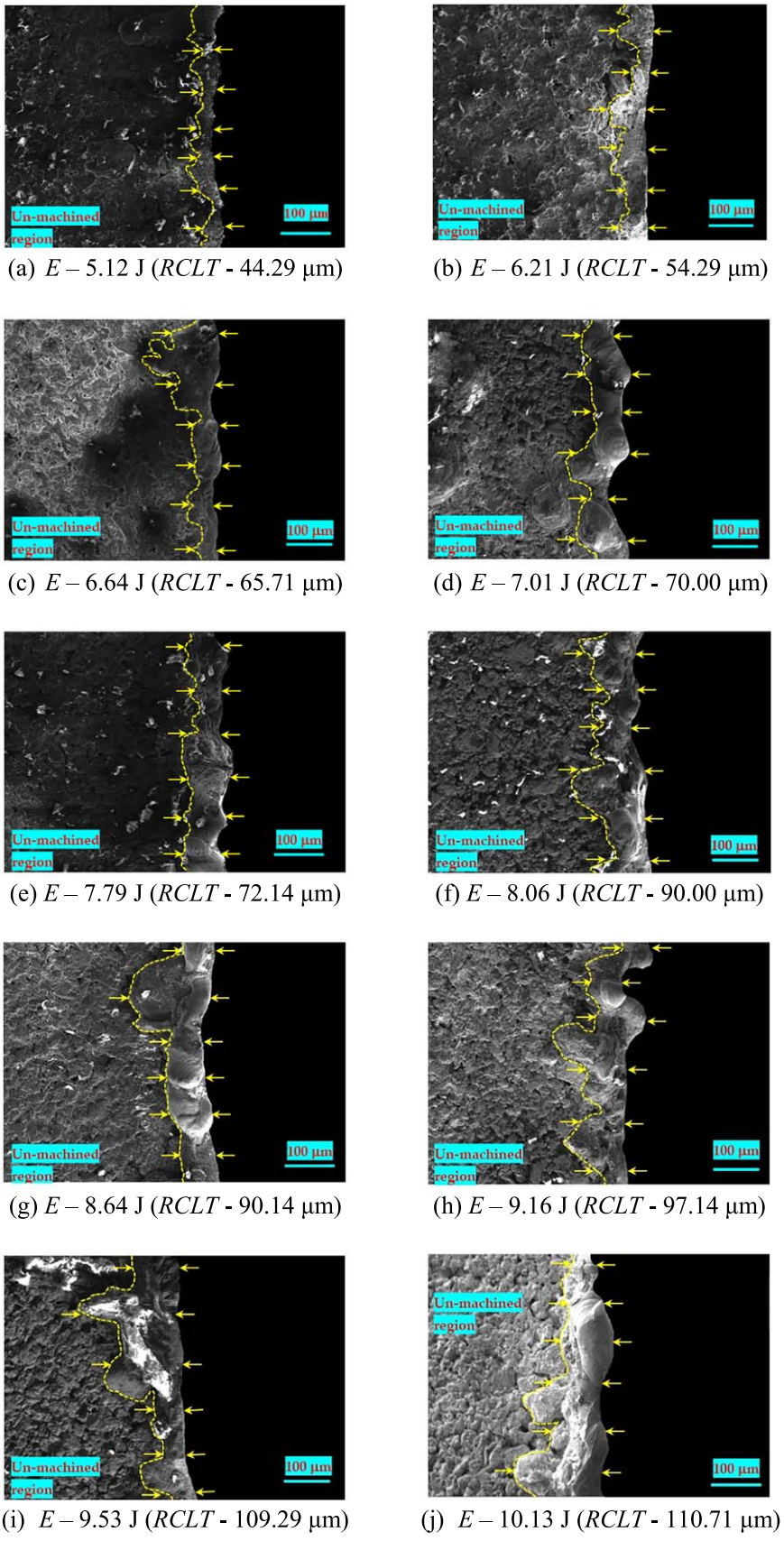

(a) E – 5.12 J (*RCLT* - 44.29 µm) (b) E – 6.21 J (*RCLT* - 54.29 µm)

(c) E – 6.64 J (*RCLT* - 65.71 µm) (d) E – 7.01 J (*RCLT* - 70.00 µm)

(e) E – 7.79 J (*RCLT* - 72.14 µm) (f) E – 8.06 J (*RCLT* - 90.00 µm)

(g) E – 8.64 J (*RCLT* - 90.14 µm) (h) E – 9.16 J (*RCLT* - 97.14 µm)

(i) E – 9.53 J (*RCLT* - 109.29 µm) (j) E – 10.13 J (*RCLT* - 110.71 µm)

Figure 8. *RCLT* of machined surface for varying *E*.

in this study is hydrocarbon oil (Technology Manual, M/s. Electronica smart ZNC) being a chemical compound of carbon and hydrogen. The localized heating during spark erosion results in decomposition of Cu and Zn; Carbon and Titanium from tool, dielectric liquid and workpiece respectively. These decomposed elements get diffused into the molten pool of electrodes. Titanium is a highly reactive material at elevated temperatures; the

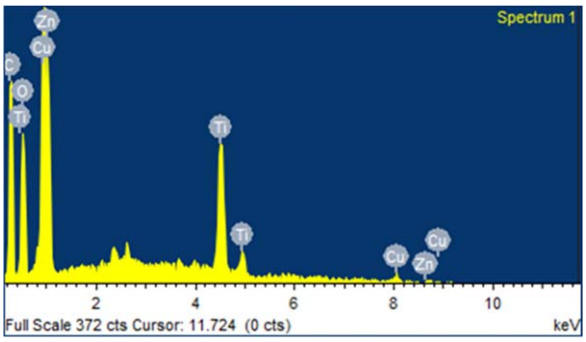

(a) E - 5.12 J

Element	Wt (%)
C K	19.08
O K	14.71
Ti K	29.18
Cu L	20.93
ZnL	16.10
Totals	100.00

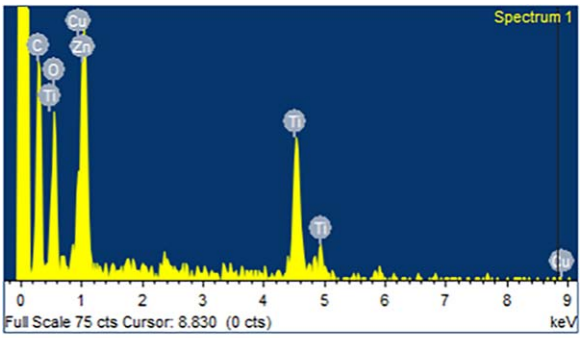

(b) E - 6.21 J

Element	Wt (%)
C K	22.24
O K	18.86
Ti K	32.92
Cu L	6.41
ZnL	19.57
Totals	100.00

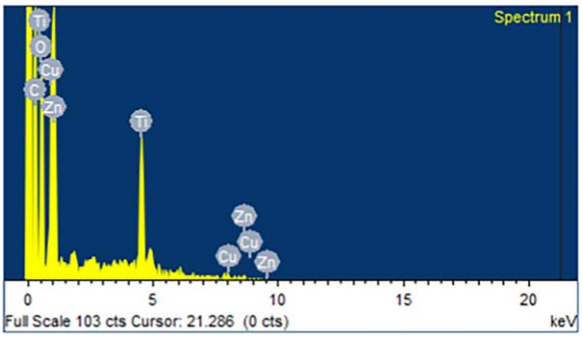

(c) E - 6.64 J

Element	Wt (%)
C K	27.13
O K	17.94
Ti K	25.93
Cu L	13.37
ZnL	15.62
Totals	100.00

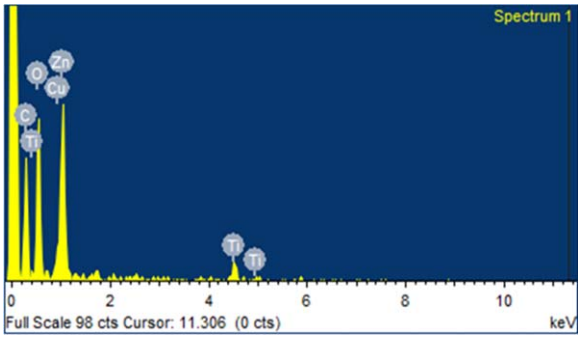

(d) E - 7.01 J

Element	Wt (%)
C K	29.80
O K	32.97
Ti K	8.63
Cu L	3.29
ZnL	25.31
Totals	100.00

Figure 9. EDS profile of machined CTF for varying E.

carbon decomposed from dielectric liquid reacts with titanium workpiece and forms titanium carbide (TiC). At the end of spark erosion, the gush of dielectric liquid cools rapidly the molten pool containing the dissolved element within it [11, 28, 33, 34]. Figure 9 shows the area energy dispersive x-ray (EDX) analysis and Energy

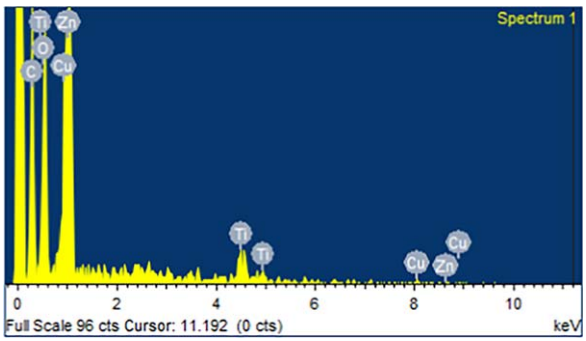

Element	Wt (%)
C K	30.77
O K	21.27
Ti K	5.93
Cu L	14.76
ZnL	27.27
Totals	100.00

(e) E - 7.75 J

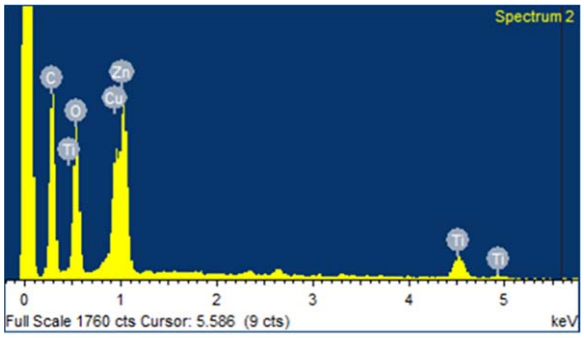

Element	Wt (%)
C K	31.09
O K	22.12
Ti K	8.92
Cu L	15.20
ZnL	22.68
Totals	100.00

(f) E - 8.64 J

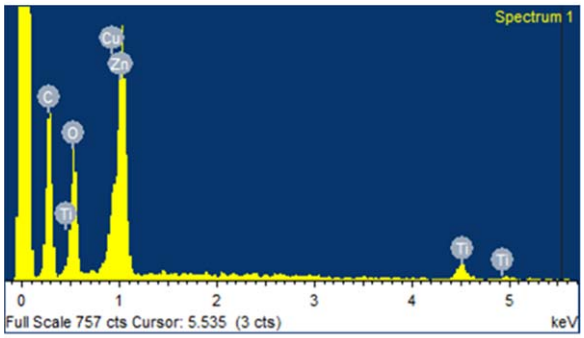

Element	Wt (%)
C K	33.40
O K	19.51
Ti K	6.12
Cu L	9.21
ZnL	31.76
Totals	100.00

(g) E - 9.16 J

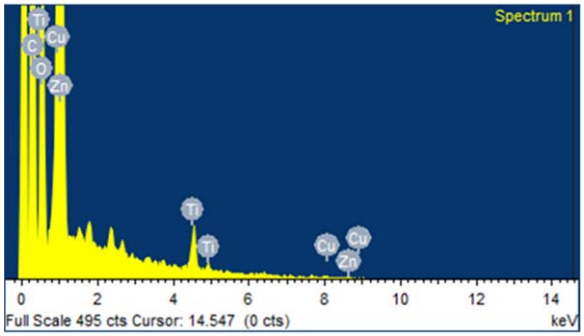

Element	Wt (%)
C K	42.54
O K	19.87
Ti K	2.90
Cu L	9.85
ZnL	24.84
Totals	100.00

(h) E - 9.53 J

Figure 9. (Continued.)

Dispersion Spectrum (EDS) revealing the presence of decomposed elements on machined workpiece measured at different E. It is observed that the pyrolytic carbon generated from dielectric medium, copper and zinc metals from tool electrode transfers into the workpiece surface. As E increases, the amount of heat produced gives rise

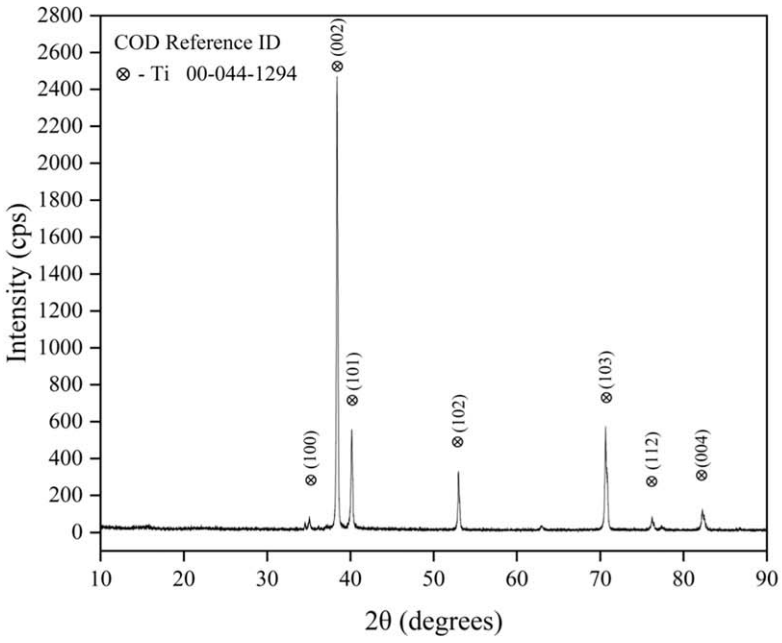

(a) Un-machined surface

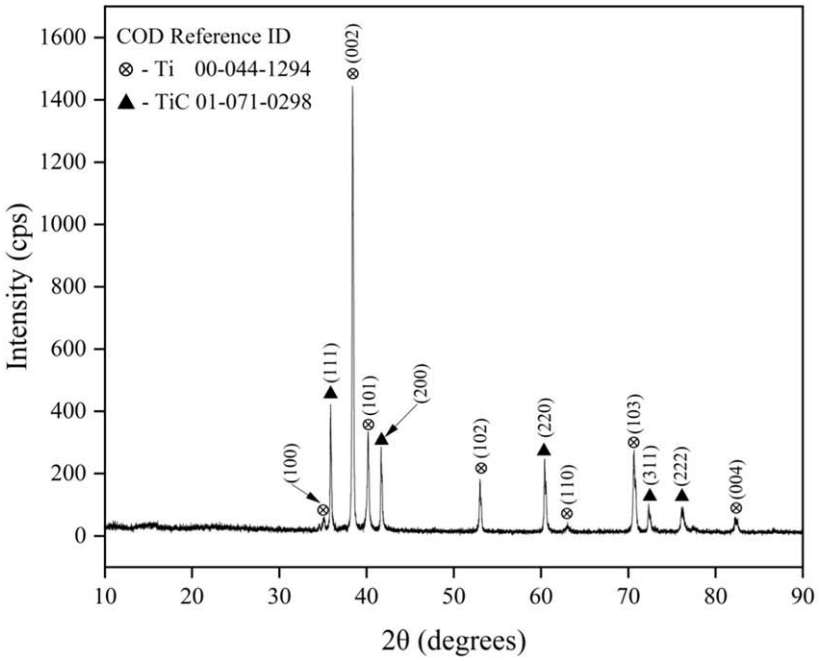

(b) Surface machined at E – 7.75 J

Figure 10. XRD profile of comparison for CTF.

to generate more pyrolytic carbon from dielectric medium. The XRD profile of surface machined at E−7.75 J reveals the presence of TiC layer as shown in figure 10. The snapshot of machined tool is presented in figure 11 revealing the deposition of decomposed carbon from the dielectric liquid. Through DSEDT it is noticed that the surface with uniform crater diameter along with TiC layer is established.

Further to assess the machined surface, the micro hardness and surface roughness for discharge energy is assessed. The micro-hardness measurement and surface roughness are measured at three different locations and is average value is presented in figures 12 and 13 respectively. It is perceived that as the E raises, the micro-hardness of machined surface increases. For a given discharge energy, during spark discharge owed to localized heating; decomposition of carbon from the dielectric liquid gets diffused into the molten pool of workpiece surface. At elevated temperatures, titanium is highly reactive; the carbon decomposed from dielectric liquid reacts with titanium workpiece and forms titanium carbide (TiC). At the end of spark erosion, the rapid flow of

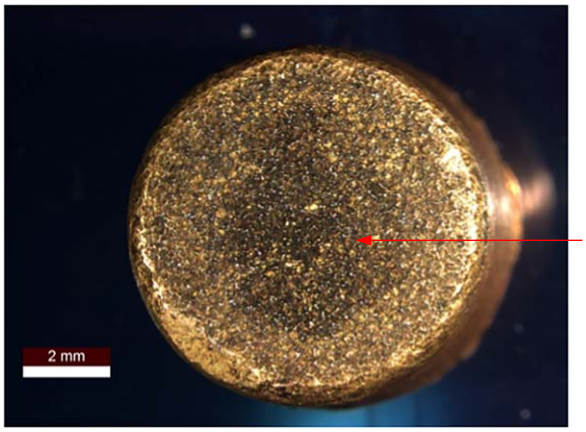

Figure 11. Snapshot of tool electrode used for machining CTF at E—6.64 J.

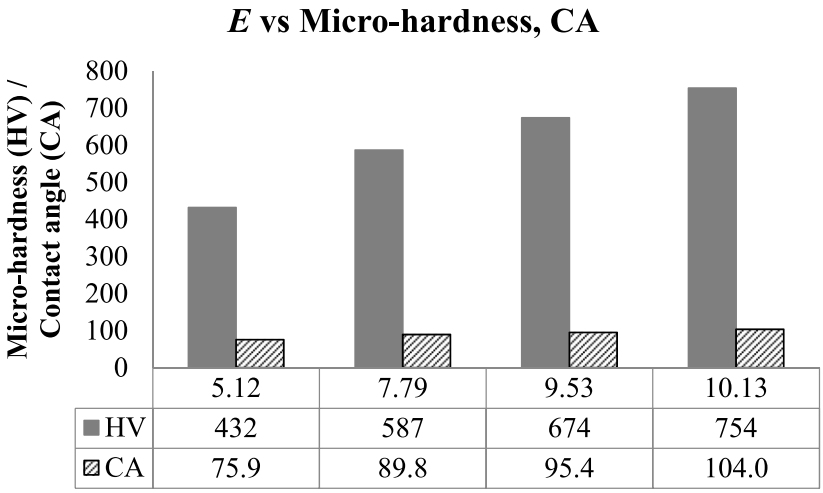

Figure 12. Effect of E on micro-hardness and contact angle.

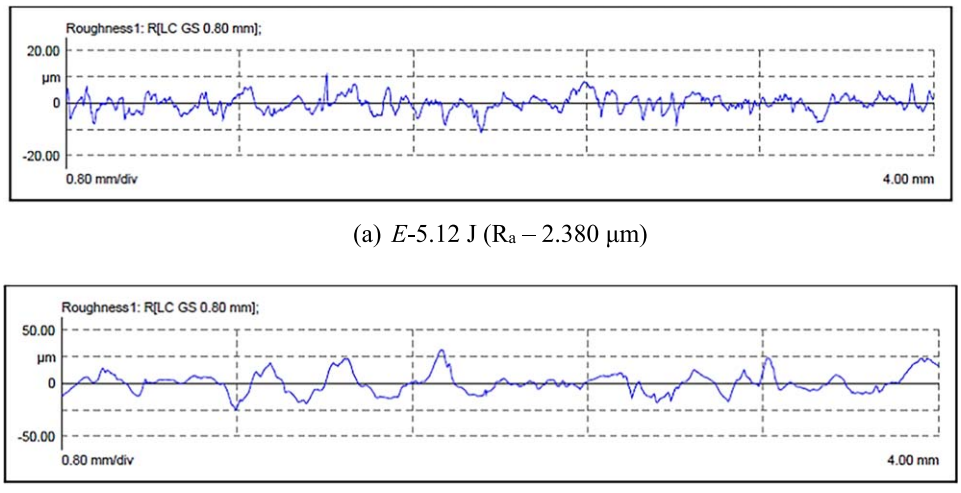

Figure 13. Significance of E on surface roughness.

dielectric liquid solidifies the molten material containing the dissolved element within it [11, 28, 33]. This resulted in formation of *RCLT* retaining the dissolved elements within. As the *E* grows, more amount of *RCLT* is formed on the machined surface containing increased amount of carbon content (wt%) which is evident from the EDS profiles presented in figure 9. The presence of TiC on the machined surface is evident from the XRD profile presented in figure 10. Therefore, the increase in *RCLT* contains more amount of TiC which resulted in raised hardness at higher discharge energy. Further the contact angle (CA) of the machined surface is measured using sessile drop method. It is perceived from figure 12, as *E* grows the CA of machined surface shifts from hydrophilic (CA $< 90°$) to hydrophobic (CA $> 90°$). Hydrophilic surfaces offer better liquid retention as compared to hydrophobic surfaces which repels liquids. In an Industry, special bearings are subjected to loading and rotation which require hardened surfaces to offer better resistance to wear along with lubricant retention property. Through this study, it is possible to produce a hardened layer along with surface behaving hydrophilic using *DSEDT* process.

The influence of varying magnitudes of *E* on surface roughness of the machined component is also analysed. On the machined surface, 2D roughness measurements are carried at three distinct locales and its average value as taken for the study. At *E* of 5.12 J, 7.79 J, 9.53 J, 10.13 J the measured average roughness (R_a) values are 3.084 μm, 5.293 μm, 6.198 μm and 7.456 μm respectively. The 2D roughness profiles of machined surfaces are presented in figure 13. It is noticed from the roughness profiles, at low *E*, the surface profile is composed of peaks and valleys of smaller magnitudes that corresponds to uniform *RCLT* formation that resulted in lower R_a value. However, the increase in *E* leads to formation of big sized crater together with non-uniform *RCLT* lead to larger magnitudes of surface profiles along with varying peaks and valleys. This resulted in surface roughness on the machined surface.

To understand further, an attempt has been made to perceive a relationship between *E*, $C_{d.avg}$ and *RCLT*. Due to the complexity involved in developing a mathematical model for DSEDT process, a well-demonstrated linear regression is adopted. In this study, by taking *E* is taken as input variable; the models for $C_{d.avg}$ and *RCLT* are expressed in equations (2) and (3) respectively

$$C_{d.avg} = 7.5106E - 10.687 \tag{2}$$

$$RCLT = 13.985E - 29.115 \tag{3}$$

The R squared value for $C_{d.avg}$ and *RCLT* are 95.71% and 96.61%. However it's difficult to obtain a correlation between the *E* and chemical alteration of the machined surfaces.

4. Conclusions

In this paper, a detailed investigation has been carried out on modifying the top surface of closed cell titanium foam during DSED texturing process. The significance of discharge time, current and discharge voltage on discharge energy is analysed. The impact of discharge energy on crater diameter, recast layer thickness and chemical alteration of machined surfaces was investigated. The following conclusions have been made from the current work.

It is observed that there is a linear proportionality between the discharge time and current, and the discharge energy. However, for higher magnitudes of current, the variation in energy is insignificant.

1. The impact of discharge energy on average crater diameter ($C_{d.avg}$) is assessed using SEM micrographs. A range of $C_{d.avg}$ varying from 44.29 μm to 110.71 μm is obtained for varying discharge energy from 5.12 J to 10.13 J respectively. The micrograph of machined surface reveals the crater overlap phenomena and the re-solidified material covers the cells present in CTF.
2. The significance of discharge energy on the *RCLT* formed on machined CTF surface is assessed. For values of energy *E* from 5.12 J–10.13 J, the *RCLT* values vary from 44.29 μm to 110.71 μm respectively.
3. The influence of discharge energy on chemical alteration of machined surface are assessed using EDS profiles. Due to pyrolytic effect, the carbon from dielectric liquid, copper and zinc from tool electrode gets transferred to machined surface. At high discharge energy, more carbon is observed on the machined surface. The XRD profile reveals the presence of titanium carbide on the machined CTF surface.
4. By increasing *E* from 5.12 J to 10.13 J, the micro-hardness grows from 432 HV to 754 HV respectively. As the *E* grows, the increased carbon (wt %) within the *RCLT* attributed to raised micro-hardness values. Also the contact angle varies from 75.9 to 104.0 degree. The R_a of the machined surface varies from 3.084 μm to 7.456 μm. By varying the *E*, it's possible to produce a component requiring improved hardness along with hydrophilic or hydrophobic surfaces.

Through this study on DSEDT of CTF, it's possible to establish a surface having improved hardness along with either hydrophilic or hydrophobic behavior by altering the discharge energy. Though the initial cell topography of CTF gets affected during DSEDT, yet the proposed work can be extended to manufacture special bearing using porous material that are subjected to loading and rotation which require hardened surfaces to offer better resistance to wear along with lubricant retention property.

Funding

'This research was funded by 'Science and Engineering Research Board (SERB)', Department of Science and Technology (DST), Government of India vide grant number ECR/2016/001326.

Conflicts of interest

'The authors declare no conflicts of interest.'

Acknowledgment

The authors express their gratitude to Science and Engineering Research Board (SERB), Department of Science and Technology (DST), Government of India, for the financial assistance provided for this research under the file number ECR/2016/001326".

Data availability statement

All data that support the findings of this study are included within the article (and any supplementary files).

ORCID iDs

Giridharan Abimannan https://orcid.org/0000-0001-7049-6687

References

[1] Aspinwall D, Wise M, Stout K, Goh T, Zhao F and El-Menshawy M 1992 Electrical discharge texturing *Int. J. Mach. Tools Manuf.* **32** 183–93
[2] Harcuba P, Bacakova L, Strasky J, Bacakova M, Novotna K and Janecek M 2012 Surface treatment by electric discharge machining of Ti-6Al-4V alloy for potential application in orthopaedics *J. Mech. Behav. Biomed. Mater.* **7** 96–105
[3] Koshy P and Tovey J 2011 Performance of electrical discharge textured cutting tools *CIRP Ann.—Manuf. Technol.* **60** 153–6
[4] Jithin S, Bhandarkar U V and Joshi S S 2019 Establishing edm as a method for inducing hydrophobicity on ss 304 surfaces *Advances in Micro and Nano Manufacturing and Surface Engineering. Lecture Notes on Multidisciplinary Industrial Engineering* ed M S Shunmugam and M Kanthababu (Springer) p. 731–40 10.1007/978-981-32-9425-7_66
[5] He Z R, Luo S T, Liu C S, Jie X H and Lian W Q 2019 Hierarchical micro/nano structure surface fabricated by electrical discharge machining for anti-fouling application *J. Mater. Res. Technol.* **8** 3878–90
[6] Bui V D, Mwangi J W and Schubert A 2019 Powder mixed electrical discharge machining for antibacterial coating on titanium implant surfaces *J. Manuf. Process.* **44** 261–70
[7] Wang H, Chi G, Jia Y, Yu F, Wang Z and Wang Y 2020 A novel combination of electrical discharge machining and electrodeposition for superamphiphobic metallic surface fabrication *Appl. Surf. Sci.* **504** 144285
[8] Matz A M, Kammerer D, Jost N and Obwald K 2016 Machining of metal foams with varying mesostructure using wire EDM *Procedia CIRP* **42** 263–7
[9] Depczynski W, Nowakowski L, Hepner P and Miko E 2017 The influence of porosity on machinability of sintered Fe foam elements *Metalurgija* **56** 364–6
[10] Klink A, Holsten M and Hensgen L 2017 Crater morphology evaluation of contemporary advanced EDM generator technology *CIRP Ann Manuf. Technol.* **66** 197–200
[11] Feng C C, Li L, Zhang C S, Zheng G M, Bai X and Niu Z W 2019 Surface characteristics and hydrophobicity of Ni-Ti alloy through magnetic mixed electrical discharge machining *Materials* **12** 388
[12] Chen X, Zhou J, Wang K and Xu Y 2022 Experimental research on single-pulse discharge crater morphology in SEAM *Mater. Manuf. Processes* **37** 664–73
[13] Bartkowiak T, Mendak M, Mrozek K and Wieczorowski M 2020 Analysis of surface microgeometry created by electric discharge machining *Materials* **13** 3830
[14] Das S, Paul S and Doloi B 2021 Assessment of the impacts of bio-dielectrics on the textural features and recast-layers of EDM surfaces *Mater. Manuf. Processes* **36** 245–55
[15] Muthuramalingam T 2019 Effect of diluted dielectric medium on spark energy in green EDM process using TGRA approach *J. Clean. Prod.* **230** 117894
[16] Bhaumik M and Maity K 2019 Effect of electrode materials on different EDM aspects of titanium alloy *Silicon* **11** 187–96
[17] Philip J T, Kumar D, Mathew J and Kuriachen B 2020 Experimental investigations on the tribological performance of electric discharge alloyed Ti–6Al–4V at 200–600 °C *J. Tribol.* **142** 061702

[18] Omer E and Gov K 2020 The effect of magnesium content on drilling of Al-Mg-Ti alloy by hole electrical discharge machining process *Proc. Inst. Mech. Eng. B J. Eng. Manuf.* **235** 125–33
[19] Sureshkumar S, Varol T, Canakci A, Kumaran T S and Uthayakumar M 2021 A review on the performance of the materials by surface modification through EDM *Int. J. Lightweight Mater Manuf.* **4** 127–44
[20] Kishi R and Yan J 2020 Electrical discharge/electrochemical hybrid machining based on the same machine and tool electrode *J. Micro. Nano-Manuf.* **8** 010906
[21] Maddu J, Karrolla B, Vuppala S and Shaik R U 2021 Formation and optimization of electrical discharge coatings using conventional electrodes *Energies.* **14** 5691
[22] Saodaen R, Janmanee P and Rodchanarowan A 2021 Characteristics of ternary metal (Cu-Ni-TiN) electrodes used in an electrical discharge machining process *Metals* **11** 694
[23] Das A and Misra J P 2016 Modelling and parametric optimisation of deposited layer thickness in electric discharge coating process *Int. J. Surf. Sci.* **10** 253–71
[24] Obwald K, Schneider S, Hensgen L, Klink A and Klocke F 2017 Experimental investigation of energy distribution in continuous sinking EDM *CIRP J. Manuf. Sci. Technol.* **19** 36–43
[25] Sambaran M, Devesh R and Giridharan A 2022 EDM of titanium foam: electrode wear rate, oversize, and MRR *Mater. Manuf. Processes* **37** 825–37
[26] Dhakar K, Kumar R, Katheria A, Nagdeve L and Kumar H 2022 Effect of various dielectric fluids on electric discharge machining (EDM): a review *J. Braz Soc. Mech. Sci. Eng.* **44** 487
[27] Giridharan A and Samuel G L 2017 Analysis on the effect of discharge energy on machining characteristics of wire electrical discharge turning process *Proc. Inst. Mech. Eng. B J. Eng. Manuf.* **230** 2064–81
[28] Dibitonto D D, Eubank P T, Patel M R and Barrufet M A 1989 Theoretical models of the electrical discharge machining process. i. a simple cathode erosion model *J. Appl. Phys.* **66** 4095–103
[29] Patel M R, Barrufet M, Eubank P T and DiBitonto D D 1989 Theoretical models of the electrical discharge machining process. II. The anode erosion model *J. Appl. Phys.* **66** 4104–11
[30] Descoeudres D, Ch. H, Walder G and Perez R 2005 Time-resolved imaging and spatially-resolved spectroscopy of electrical discharge machining plasma *J. Phys. D: Appl. Phys.* **38** 4066–73
[31] Zhang Y, Liu Y, Shen Y, Ji R, Li Z and Zheng C 2014 Investigation on the influence of dielectrics on the material removal characteristics of EDM *J. Mater. Process. Technol.* **214** 1052–61
[32] Hinduja S and Kunieda M 2013 Modelling of ECM and EDM processes *CIRP Ann: Manuf. Technol.* **62** 775–97
[33] Chen S L, Yan B H and Huang F Y 1999 Influence of kerosene and distilled water as dielectrics on the electric discharge machining characteristics of Ti–6A1–4V *J. Mater. Process. Technol.* **87** 107–11
[34] Holsten M, Koshy P, Klink A and Schwedt A 2018 Anomalous influence of polarity in sink EDM of titanium alloys *CIRP Ann.* **67** 221–4